

1 **Advance prediction of coastal groundwater levels with temporal**  
2 **convolutional and long short-term memory networks**

3 Xiaoying Zhang<sup>a,b</sup>, Fan Dong<sup>a,b</sup>, Guangquan Chen<sup>c</sup>, Zhenxue Dai<sup>a,b\*</sup>

4 <sup>a</sup> Institute of Intelligent Simulation and Early Warning for Subsurface Environment,  
5 Jilin University, Changchun, China

6 <sup>b</sup> College of Construction Engineering, Jilin University, Changchun, China

7 <sup>c</sup> Key Laboratory of Marine Sedimentology and Environmental Geology, First  
8 Institute of Oceanography, State Oceanic Administration, Qingdao, China

9 \* Correspondence: Zhenxue Dai, [dzx@jlu.edu.cn](mailto:dzx@jlu.edu.cn)

10

11 **Highlights**

- 12 • TCN- and LSTM-based models were proposed to predict groundwater levels in a  
13 coastal aquifer
- 14 • Tidal, precipitation, and groundwater levels were utilized as input data in the  
15 networks
- 16 • In advance 1- day, 3-, 7-, and 15-day groundwater levels were predicted with the  
17 highest accuracy of 1-day-lead prediction
- 18 • The TCN-based model slightly outperformed the LSTM-based model in accuracy  
19 but less efficiency

20

21 **Abstract**

22 Prediction of groundwater level is of immense importance and challenges for coastal  
23 aquifer management with rapidly increasing climatic change. With the development of  
24 artificial intelligence, data-driven models have been widely adopted in hydrological  
25 process management. However, due to the limitation of network framework and  
26 construction, they are mostly adopted to produce only a one-time step in advance. Here,  
27 the temporal convolutional network (TCN) and long short-term memory (LSTM) based

28 models were developed to predict groundwater levels with different leading periods in  
29 a coastal aquifer. The beginning hourly-monitored ten-month data in two monitoring  
30 wells were used for model training and testing, and the data of the following three  
31 months were used as prediction with 24, 72, 180, and 360 timesteps (1-day, 3-, 7-, and  
32 15-days) in advance. The historical precipitation and tidal level data were incorporated  
33 as input data. For the one-step prediction of the two wells, the calculated  $R^2$  of the TCN-  
34 based models' values were higher and the RMSE values were lower than that of the  
35 LSTM-based model in the prediction stage with shorter running times. For the advanced  
36 prediction, the model accuracy decreased with the increase of the advancing period  
37 from 1-day to 3-, 7-, and 15-days. By comparing the simulation accuracy and efficiency,  
38 the TCN-based model slightly outperformed the LSTM-based model but was less  
39 efficient in training time. Both models showed great ability to learn complex patterns  
40 in advance using historical data with different leading periods and had been proven to  
41 be valid localized groundwater level prediction tools in the subsurface environment.

42

43 **Keywords:** Groundwater level prediction; Coastal aquifer; Temporal convolutional  
44 networks; Long Short-Term Memory

45

46

47

48

## 49 **1 Introduction**

50 As the economic development and population escalate in the coastal area, the fresh  
51 groundwater needs continue to mount, and seawater intrusion has posed a great threat  
52 to the availability of portable water resources globally (Baena-Ruiz et al., 2018). In the  
53 United States, Mexico, Canada, Australia, China, India, South Korea, Italy, and Greece,  
54 with dense population, many coastal aquifers have experienced salinization caused by  
55 seawater intrusion (Barlow and Reichard, 2009; Park et al., 2011; Pratheepa et al., 2015;  
56 Zhang et al., 2017; Lu et al., 2013). Protection projects such as aquifer replenishment  
57 can be constructed to alleviate seawater intrusion by artificially increasing groundwater  
58 recharge in the aquifer than what occurs naturally (Abdalla and Al-Rawahi, 2012; Lu  
59 et al., 2019). The replenishment programs have been operated in the developed areas  
60 such as Perth, Western Australia, and California, USA (Garza-Díaz et al., 2019). The  
61 infrastructures tend to be costly and out of reach for many developing countries. A  
62 reliable seawater intrusion monitoring and the predicting system is still essential and is  
63 recognized as the most effective way of keeping fresh water from seawater  
64 contamination (Xu and Hu, 2017).

65 In the past several decades, conventional numerical models have been widely  
66 utilized to simulate and predict groundwater fluctuation dynamics and chemical  
67 variations (Batelaan et al., 2003; Dai et al., 2020; Huang et al., 2015; Li et al., 2002).  
68 However, the difficulty of acquiring extensive hydrological and geological data and  
69 setting reasonable boundaries limits its application to seawater intrusion management.  
70 Meanwhile, the method is not suitable for simultaneously adopting updated monitoring

71 data and producing real-time prediction. Under such circumstances, where the data  
72 source is scarce, artificial intelligence technology has been proposed in groundwater  
73 dynamic predictions. Artificial neural network (ANN) has been greatly improved and  
74 has become a robust tool for dealing with groundwater problems where the flow is  
75 nonlinear and highly dynamic in nature (Maier and Dandy, 2000). The conventional  
76 network model generally has defects such as high computational complexity, slow  
77 training speed, and failure in retaining historical information, thus is hard to be enrolled  
78 in the long-term time-series prediction (Cannas et al., 2006; Mei et al., 2017). To solve  
79 this problem, researchers upgraded the conventional networks by integrating them with  
80 methods like a genetic algorithm (Danandeh Mehr and Nourani, 2017; Ketabchi and  
81 Ataie-Ashtiani, 2015), singular spectrum (Sahoo et al., 2017), and wavelet transform  
82 (Gorgij et al., 2017; Seo et al., 2015; Zhang et al., 2019). Singular spectrum analysis  
83 and wavelet transform can help to preprocess the time-series data before they are put  
84 into the neural networks to improve prediction accuracy and efficiency.

85         With computing capacity development, deep learning (DL) has emerged as a very  
86 powerful time-series prediction method. DL models are particularly suitable for big data  
87 time-series because they can automatically extract complex patterns without feature  
88 extraction preprocessing steps (Torres et al., 2019). However, the generally fully  
89 connected networks are not effective in capturing the temporal dependence of time  
90 series (Senthil Kumar et al., 2005). Therefore, more specialized DL models, such as  
91 recurrent neural networks (RNN) (Rumelhart et al., 1986) and convolutional neural  
92 networks (CNN) (Lecun et al., 1998) have been adopted in the field of time-series

93 prediction (Feng et al., 2020). Different from the back-propagation (BP) neural network  
94 that the information flows from the input to the output layer in one direction, the RNN  
95 preserves the information from the previous step as input to the current step with loops  
96 (Coulibaly et al., 2001). This allows the RNN to handle time-series and other sequential  
97 data but generally is not straightforward for a long-term calculation in practice (Bengio  
98 et al., 1994). Therefore, the enhanced RNN model, long short-term memory (LSTM) is  
99 proposed and capable of processing high variable-length sequences even with millions  
100 of data points (Fischer and Krauss, 2018; Kratzert et al., 2019) . As one of the best deep  
101 neural network model in time-series predicting, the LSTM has been widely used in the  
102 prediction of temporal variations such as stock market predictions (Fischer and Krauss,  
103 2018), rainfall-runoff (Kumar Dubey et al., 2021), and groundwater level (Solgi et al.,  
104 2021). Despite substantial progress in hydrology prediction, these networks still have  
105 issues of low training efficiency and low accuracy (Zhan et al., 2022).

106 More recently, a variant of the CNN architecture known as temporal convolutional  
107 networks (TCN) has acquired popularity (Bai et al., 2018). The prominent characteristic  
108 of TCN is its ability to capture long-term dependencies without information loss (Cao  
109 et al., 2021). Meanwhile, it joints a residual block structure to fix the disappearance of  
110 the gradient in the deep network structure (Chen et al., 2020). With proper  
111 modifications, the TCN is quite genetic and easily to be used to build a very deep and  
112 extensive network in sequence modeling. In earth science, the TCN has been  
113 successfully applied to time-series prediction tasks, including multivariate time-series  
114 predicting for meteorological data (Wan et al., 2019), probabilistic predicting (Chen et

115 al., 2020) and wind speed predicting (Gan et al., 2021). Researchers suggest that the  
116 TCN convincingly has the advantage in popular deep-learning models across a broad  
117 range of sequence modeling tasks (Borovykh et al., 2019; Chen et al., 2020; Wan et al.,  
118 2019). Another important subject is that these networks are mostly used to predict  
119 variables in only one step, which is not enough for the prediction of hydrology  
120 information in management. Researches have adopted the method to predict the trends  
121 of ENSO and sea temperature (Yan et al.,2020; Jian et al., 2021). However, the potential  
122 of TCN has not been investigated in the sequencing model of the hydrogeology field.  
123 Therefore, it is worthy to explore their prediction abilities in leading periods.

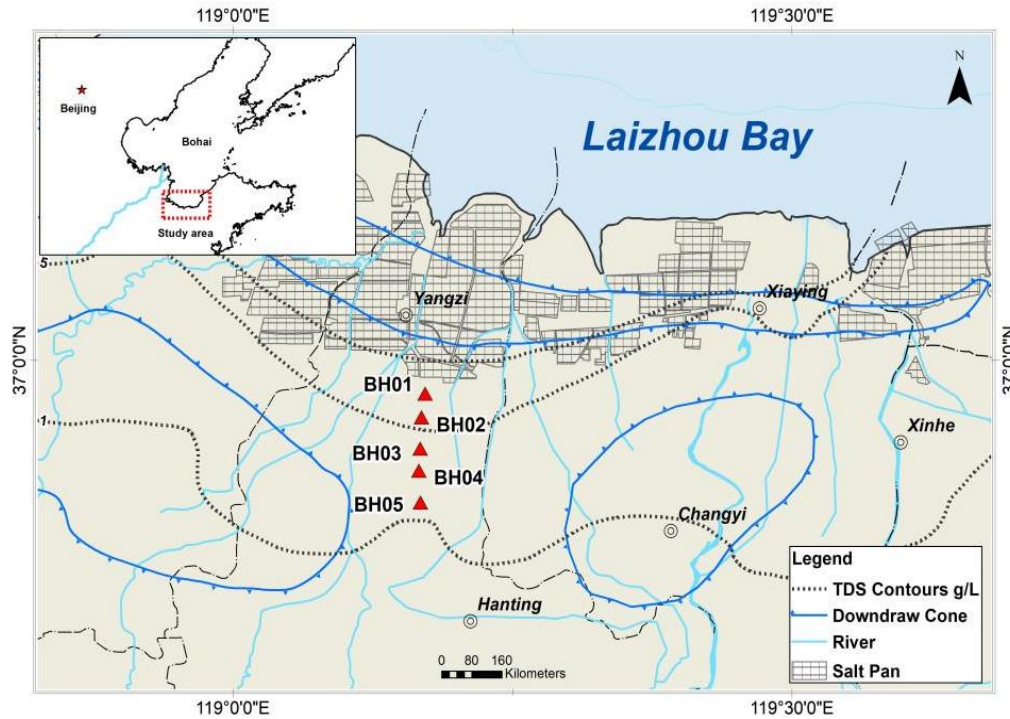
124 The objective of this study is to develop real-time advance prediction climate-  
125 hydro hybrid data-driven models of groundwater level in the coastal aquifer based on  
126 TCN and LSTM. The hourly processed tidal, precipitation with groundwater level data  
127 in monitoring wells of Laizhou Bay are utilized to train the model and predict the  
128 groundwater level in a period of 1-day, 3-, 7-, and 15-days. The two models were further  
129 compared in view of accuracy and efficiency. The rest of the paper is organized as  
130 follows. Sec. 2 introduces the study area and observational data. Sec. 3 illustrates the  
131 detailed concepts of TCN and LSTM, the experimental model settings and model  
132 evaluation criteria. Sec. 4 presents the predicted results and discussions. Finally, the  
133 paper is concluded in Sec. 5.

## 134 **2 Study area and data processing**

### 135 **2.1 Site description**

136 The study area is located on the south coast of Laizhou Bay, along the Yangzi to

137 Weifang section in the Shandong province of China (Fig. 1). The Laizhou Bay has been  
138 one of the earliest and most seriously affected areas by seawater intrusion since the  
139 1970s in China (Han et al., 2014; Zeng et al., 2016). The area is a coastal plain, which  
140 contains a series of Cretaceous to modern sediments that cover the Paleozoic basement.  
141 The sedimentary facies of coastal aquifer are alluvium, pluvial, and marine sediments  
142 from south to north (Han et al., 2011). According to the research of (Xue et al., 2000),  
143 there have been three seawater intrusion and regression events in the sea area of  
144 Laizhou Bay since the upper Pleistocene. The transgression in the early upper  
145 Pleistocene formed the third marine aquifer containing sedimentary water. This brine  
146 was formed by evaporation and concentration of ancient seawater and re-dissolution  
147 and mixing of salt (Dai and Samper, 2006; Zhang et al., 2017). The monitoring wells  
148 BH01-BH05 are distributed in the study area along a cross-section perpendicular to the  
149 coastline. Among the wells, wells BH01 and BH05 have relatively integrated data in  
150 time and are distributed on the two sides of the cross profile with distinguished annual  
151 variation patterns, which are selected as examples for the developed models.



152

153 Figure 1. Schematic figure of the study area with monitoring wells BH01-BH05.

154 **2.2 Data collection and pre-processing**

155 The precipitation and tidal level are selected as the primary factors to affect the  
 156 groundwater dynamics in the coastal area. The data in the period of 2011 to 2012 with  
 157 groundwater level observations of two wells are combined as the input of the deep  
 158 learning models. A total of 28,836 data items are collected for monitoring wells. The  
 159 variations of groundwater level and tidal level with precipitation are shown in Figure 2.  
 160 The rainfall is concentrated from June to September and in shortage from December to  
 161 April. The tide in the study area is irregular, mixed with a semi-diurnal variation. In the  
 162 experiments, ten months of data from October 2011 to July 2012 is first extracted for  
 163 model training and testing. The rest of the data from August 2012 to October 2012 is  
 164 used to test model prediction accuracy.

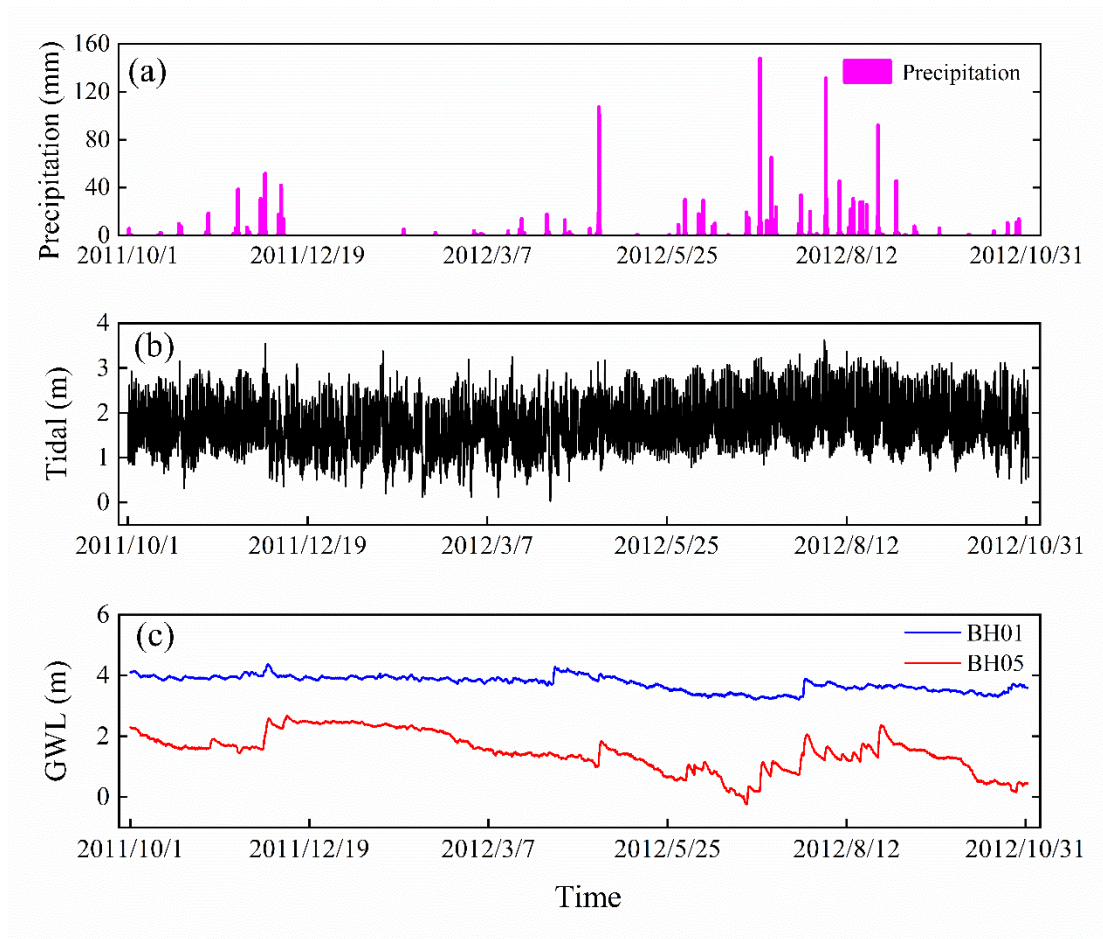
165 In addition, the magnitudes of meteorological and hydrological variables have



166 obvious temporal variations. To reduce the negative impact on the model learning  
 167 ability, especially on the speed of gradient descent, all variables are normalized to  
 168 ensure that they remain at the same scale (Kratzert et al., 2019). This pre-processing  
 169 method ensures the stable convergence of parameters in the developed TCN- and  
 170 LSTM-based models and improve the simulation accuracy of the model. The  
 171 normalization formula is as follows:

$$172 \quad x'_i = \frac{x_i - x_{min}}{x_{max} - x_{min}} \quad (1)$$

173 where  $x_i$  represents the original data in time  $i$ .  $x_{max}$  and  $x_{min}$  are the maximum and  
 174 minimum variable values. The output of the network is retransformed to obtain the final  
 175 groundwater level prediction, which is an inverse data scaling process.



176  
 177 Figure 2. Time-series of the variables in the study, including (a) precipitation, (b) tide,

178 (c) groundwater level (GWL).

## 179 **3 Methodology**

### 180 **3.1 Temporal Convolutional Network**

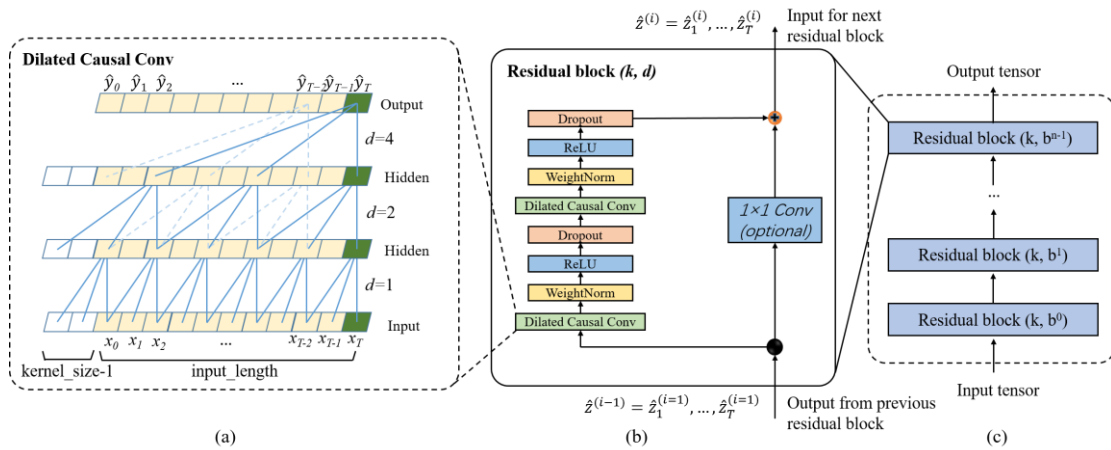
181 The TCN is first proposed for video action segmentation and detection by  
182 hierarchically capturing intermediate feature presentations. Then the term is extended  
183 for sequential data for a wide family of architectures with generic convolution (Bai et  
184 al., 2018; Lea et al., 2017). Suppose that we have an input hydro-climate sequence at  
185 different times  $x_0, \dots, x_T$ , the goal of the modeling is to predict the corresponding  
186 groundwater level as outputs  $y_0, \dots, y_T$  at each time. The problem could transfer to build  
187 a network  $f$  that minimizes the function loss between observations and actual network  
188 outputs  $L[(y_0, \dots, y_T), (\hat{y}_0, \dots, \hat{y}_T)]$ , where  $\hat{y}_0, \dots, \hat{y}_T = f(x_0, \dots, x_T)$ . Currently, a typical  
189 TCN consists of dilated, causal 1D full-convolutional layers with the same input and  
190 output lengths. With TCN, the prediction  $y_t$  depends only on the data from  $x_0$  and  $x_t$  and  
191 does not include the future data from  $x_t$  and  $x_T$  (Yan et al., 2020). With the three key  
192 components of TCN, it has two distinguishing characteristics: (1) the TCN is able to  
193 map the same length of output as the input sequence as in RNN; (2) the convolution  
194 involved in TCN is causal, eliminating the influence of future information on the output.

#### 195 3.1.1 Causal Dilated Convolutions

196 In the TCN, the first advantage is accomplished by a 1D full-convolutional network  
197 (FCN) architecture. Different from the traditional CNN, the FCN transforms the fully  
198 connected layers into the convolutional layers for the last layers, preserving the same  
199 length of output as that of the input (Long et al., 2015). As shown in Fig. 3a, the lengths

200 of the input, the hidden and the output layers are the same in the FCN. Some zero  
 201 padding is needed in this step by adding additional zero-valued entries with a length of  
 202 kernel size-1 in each layer. The kernel size is the number of successive elements that  
 203 are used to produce one element in the next layer.

204 To avoid information leakage from the future (after time  $t$ ), the TCN uses causal  
 205 convolution instead of standard convolution, where only the elements at or before time  
 206  $t$  in the previous layer are adopted into the mapping of the output at time  $t$ . Further, the  
 207 dilated convolution is employed to capture long-term historical information by skipping  
 208 a given step size (dilation factor  $d$ ) in each layer. For example, the dilation factor  $d$   
 209 increases from 1 to 4 with the evolution of the network depth ( $n$ ) in an exponentially  
 210 increasing pattern. In this way, a very large receiving domain is created and all the  
 211 historical records in the input can be involved in the prediction model with a deep  
 212 network.



213 (a) (b) (c)

214 Figure 3. Architectural elements in the proposed TCN. (a) the structure of causal dilated  
 215 convolution; (b) the TCN residual block. A 1x1 convolution is added when residual  
 216 input and output have different dimensions; (c) framework of residual connection in the

217 TCN.

### 218 3.2.2 Residual Connections

219 In a high dimensional and long-term sequence, the network structure could be very  
220 deep with increasing complicity and cause a vanishing gradient. To solve this issue, a  
221 residual block structure is introduced to replace the simple 1D causal convolution layer  
222 so that the designed TCN structure is more generic (He et al., 2016). The residual block  
223 in a TCN is represented in Fig. 3b. It has two convolutional layers with the same kernel  
224 size and dilation factor and non-linearity. To solve non-linear models, the rectified  
225 linear unit (ReLU) is added to the top of the convolutional layer (Nair and Hinton, 2010).  
226 The weight normalization is applied between the input of hidden layers (Salimans and  
227 Kingma, 2016). Meanwhile, a dropout is added after each dilated convolution for  
228 regularization (Srivastava et al., 2014). For all connected inner residual blocks, the  
229 channel widths of input and output are consistent. But the width may be different  
230 between the input of the first convolutional layer of the first residual block and the  
231 output of the second convolutional layer of the last residual block. Therefore, a  $1 \times 1$   
232 convolution is added in the first and last residual block to adjust the dimensions of the  
233 residual tensor to the same. The output of the residual block is represented by  $\hat{Z}^{(i)}$  for  
234 the  $i^{\text{th}}$  block.

### 235 3.2.3 Structure of TCN

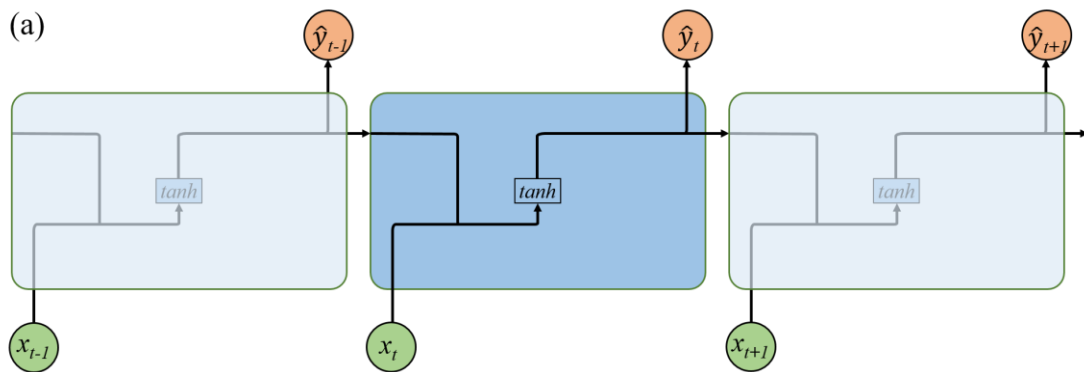
236 A complete structure of TCN is illustrated in Fig.3c. It contains a series of  
237 proceeding residual blocks. The structural characteristics make TCN a deep learning  
238 network model very suitable for complex time-series prediction problems (Lara-

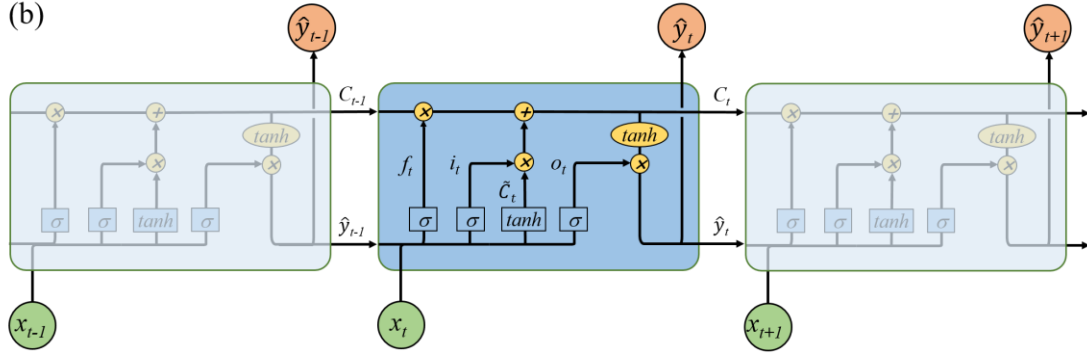
239 Benítez et al., 2020). The main advantage of TCN is that, similar to RNN, they have  
240 flexible receptive fields and can deal with various length inputs by sliding one-  
241 dimensional causal convolution kernel. Furthermore, because TCN shares a  
242 convolution kernel and has parallelism, it can process long sequences in parallel instead  
243 of sequential processing like RNN, so it has lower memory usage and shorter  
244 computing time than a cyclic network. Moreover, RNN often has the problems of  
245 gradient disappearance and gradient explosion, which are mainly caused by sharing  
246 parameters in different periods, while TCN uses a standard backpropagation-through-  
247 time algorithm (BPTT) for training, so there is little gradient disappearance and  
248 explosion problem (Pascanu et al., 2012). The detailed mathematical calculation and  
249 associated information of the TCN architecture are referred to (Bai et al., 2018).

### 250 **3.2 Long Short-Term Memory network**

251 LSTM is a special RNN model explicitly designed for long-term dependence  
252 problems. As shown in Fig. 4a, the RNN has a series of repeating modules that are  
253 recursively connected in the evolution direction of the sequence. The chain-like  
254 structure permits the RNN to retain important information in a “tanh” layer and produce  
255 the same length of output  $\hat{y}_t$  as input  $x_t$ . However, the short-length “remember time” is  
256 not enough for groundwater prediction. Especially for our hourly recorded data, a  
257 maximum step of about ten reported by Bengio et al. (1994) is unable to count the effect  
258 of annual, seasonal, and even daily groundwater variation. Different from the simple  
259 layer in the RNN, the LSTM has a more complicated repeating module with four  
260 interacting layers.

261 The core idea of LSTM is the special structure to control the cell state in the  
 262 module as shown in Fig. 4b. It includes a cell and an input gate  $i_t$ , a forget gate  $f_t$ , and  
 263 an output gate  $o_t$ . The information can directly flow down along cells  $C$  without critical  
 264 changes, therefore, preserving long-term history messages (Zhang et al., 2018b). The  
 265 three gates control which data in a sequence is important to keep or throw away, and  
 266 protect the relevant information passed down in the cell to make predictions. The forget  
 267 gate  $f_t$  has a sigmoid layer to determine which information is discarded with a value  
 268 between 0 and 1. The lower the value, the less information is added to the cell state  
 269 (Ergen and Kozat, 2018). Opposite the forget gate, the input gate  $i_t$  decides what  
 270 information to retain in the cell state. It is composed of two parts: a sigmoid layer and  
 271 a tanh layer. The two layers are combined to govern which values will be updated by  
 272 generating a new candidate value  $\tilde{C}_t$ . The old cell state  $C_{t-1}$  can then be updated into  
 273 the new cell state  $C_t$  with a weighted function. Finally, the output gate  $o_t$  determines  
 274 what parts of the cell state should be passed on to the next hidden state. The detailed  
 275 calculation of the LTSM can be referenced to (Lea et al., 2016).





277

278

Figure 4. Graphical representation for (a) chain-like structure of the RNN by

279

assigning  $x_t$  and  $\hat{y}_t$  as input and output. The self-connected hidden units allow

280

information to be passed from one step to the next; (b) LSTM's memory block based

281

on RNN. The hidden block includes three gates (input  $i_t$ , forget  $f_t$ , output  $o_t$ ) and a cell

282

state to select and pass the historical information.

283

### 3.3 Experimental study

284

The TCN- and LSTM-based models were developed separately for monitoring

285

wells BH01 and BH05. Due to the high complexity of the DL models, setting

286

appropriate hyper-parameters for the developed networks is very important. Here, the

287

impact of the size of the input window, the epoch number, and the batch size was tested

288

with different convolutional architectures over the monitoring data (Lara-Benítez et al.,

289

2020). The learning dataset is first divided into two parts: 80% of the time-series data

290

is used as the training set, and 20% of the data is utilized as the testing set. The effect

291

of different splitting strategies is further tested in section 4. With the increase of the

292

epoch numbers, the curve gradually approaches the optimal fitting state from the initial

293

non-fitting state, but too many epochs frequently lead to over-fitting of the neural

294

network (Afaq and Rao, 2020). Meanwhile, the number of iterations generally increases

295

for updating weights in the neural network. Therefore, the number of epochs from 0 to

296 300 is evaluated. Batch size represents the number of samples between model weight  
297 updates (Kreyenberg et al., 2019). The value of the batch size often is set between 1  
298 and hundreds. A larger batch size often leads to faster convergence of the model but  
299 may lead to less ideal of the final weight set. To find the best balance between memory  
300 efficiency and capacity, the batch size should be carefully set to optimize the  
301 performance of the network model. Besides these parameters, the number of filters in  
302 the TCN-based and the hidden nodes in the LSTM-based model was as well tested  
303 within reasonable ranges.

304 The 1-day, 3-, 7-, and 15-days leading prediction experiments were further  
305 conducted to test the capacity of DL methods in predicting long-term groundwater  
306 levels in the coastal aquifer. To eliminate the randomness of model training, all  
307 experiments were repeated 5 times and the average values of each index were compared.  
308 In all experiments, the average absolute error (MAE) has been used as the loss function  
309 of networks (Lara-Benítez et al., 2020). The Adam optimizer has an adaptive learning  
310 rate, which can improve the convergence speed of deep networks, which has been used  
311 to train the models (Kingma and Ba, 2015).

### 312 **3.4 Evaluation of model performance**

313 Two evaluation metrics, coefficient of determination ( $R^2$ ) and root mean square  
314 error (RMSE) are selected to quantify the goodness-of-fit between model outputs and  
315 observations (Zhang et al., 2020). The two criteria are calculated using the following  
316 equations:

$$317 \quad RMSE = \sqrt{\frac{1}{N} \sum_{i=1}^N (h_i - y_i)^2} \quad (1)$$



318 
$$R^2 = \frac{\sum_{i=1}^N (h_i - \bar{h})^2 - \sum_{i=1}^N (h_i - y_i)^2}{\sum_{i=1}^N (h_i - \bar{h})^2} \quad (2)$$

319 where  $h_i$  is the observed groundwater level at time  $i$ ,  $y_i$  is the network prediction values  
320 at time  $i$ ,  $\bar{h}$  is the mean of the observed groundwater levels, and  $n$  is the number of  
321 observations. RMSE measures the prediction precision which creates a positive value  
322 by squaring the errors. The RMSE score is between  $[0, \infty]$ . If the RMSE approaches 0,  
323 the model prediction is ideal.  $R^2$  measures the degree of model replication results,  
324 ranging between  $[-\infty, 1]$ . For the optimal model prediction, the score of  $R^2$  is close to  
325 1.

## 326 **4 Results and discussions**

### 327 **4.1 Hyper-parameter trial experiments**

#### 328 4.2.1 Experiments of the TCN-based model

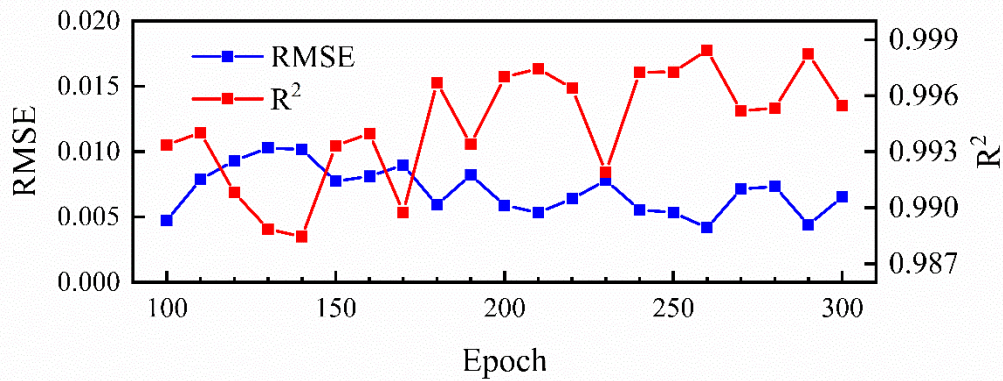
329 The TCN-based model was built on the Keras platform using TensorFlow of python  
330 as the backend. Taking the groundwater level prediction data set in well BH01 as an  
331 example, the trials were set up with a variety combination of different hyper-parameters  
332 in the TCN-based model as illustrated in Table 1. With the fixed number of epochs, the  
333 simulation results of 32 filters were better than that of 16 and 64 filters. Meanwhile,  
334 under the condition of 32 filters, the accuracy of the model decreased with the  
335 increasing batch size. The results of the 16 batch size were better than that of 32 and 64  
336 batches. Based on the above experimental results, the influence of different numbers of  
337 epochs on the simulation was further explored with the filters was 32 and the batch size  
338 was 16, as shown in Fig. 5. The overall results of the model were improved when the  
339 number of epochs increased from 100 to 190 though the variation was not strictly linear,

340 and the variations became stable with minor fluctuations when the number of epoch  
 341 exceeded 200.

342 Table 1. The RMSE and  $R^2$  values between the observed and predicted groundwater  
 343 levels in well BH01 with different numbers of epochs, different numbers of filters, and  
 344 different batch sizes. The bold values represent the optimal hyper-parameters with the  
 345 smallest RMSE and the highest  $R^2$  scores in the TCN-based model.

Epoch	Filters	Batch size	RMSE(m)	$R^2$	Time(min)
100	32	16	0.0182	0.9904	1.29
		32	0.0117	0.9876	1.05
		64	0.0117	0.9875	0.78
200	16	16	0.0078	0.9946	2.41
		32	0.0068	0.9959	1.75
		64	0.0090	0.9942	1.19
200	32	16	0.0059	0.9970	2.58
		32	0.0075	0.9948	2.01
		64	0.0082	0.9938	1.51
200	64	16	0.0125	0.9906	3.68
		32	0.0101	0.9907	3.21
		64	0.0157	0.9775	2.76
300	32	16	0.0065	0.9955	3.8
		32	0.0076	0.9946	3.01
		64	0.0099	0.9904	2.22

346



347

348 Figure 5. The variation of RMSE and R<sup>2</sup> values between the observed and predicted  
 349 groundwater levels of well BH01 with the increasing number of the epoch when the  
 350 number of filters is 32 and the batch size is 16.

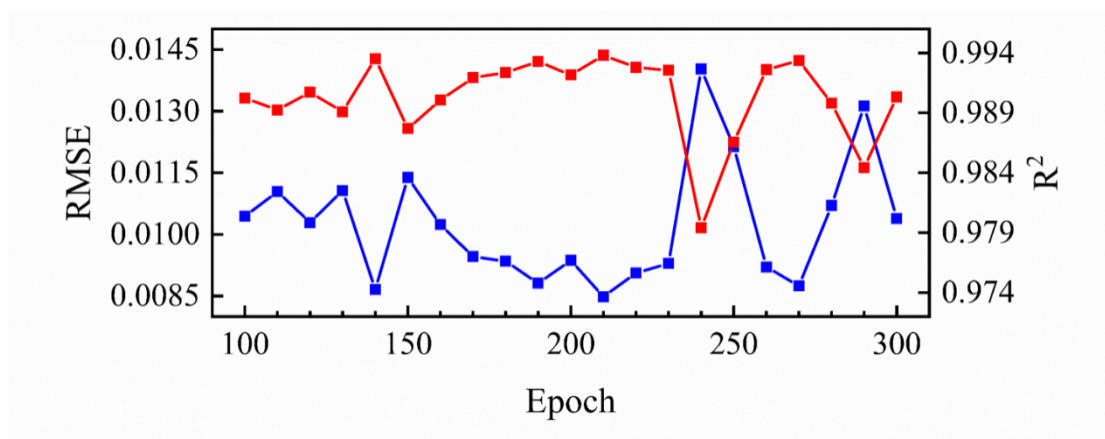
#### 351 4.2.2 Experiments of the LSTM-based model

352 The number of epochs and hidden nodes are two key parameters affecting the  
 353 simulation accuracy of LSTMs (Zhang et al., 2018a). Different hyper-parameter  
 354 combinations were tested as well as in the proposed TCN-based model with  
 355 groundwater levels in well BH01. The RMSE, R<sup>2</sup> and running time are shown in Table  
 356 2. With a fixed number of hidden nodes, the results of 100 and 200 epochs were better  
 357 than that in the 300 epochs experiment. A detailed variation of RMSE and R<sup>2</sup> values  
 358 with the increasing number of hidden nodes and epochs is further illustrated in Fig. 6.  
 359 The figure shows that the RMSE and R<sup>2</sup> have a decreasing and increasing trend  
 360 separately when the number of epochs is greater than 150, but is reversed when it is  
 361 larger than 240. The variations of RMSE and R<sup>2</sup> with increasing hidden nodes have  
 362 similar changes as shown in Table 2. Though an insufficient number of neurons may  
 363 decrease the learning ability of the network, the results indicate that increasing training  
 364 hyper-parameters may not be necessary to ensure better prediction.

365 Table 2. The RMSE and  $R^2$  values between the observed and predicted groundwater  
 366 levels in well BH01 with different numbers of epochs and hidden nodes. The bold  
 367 values represent the optimal hyper-parameters used in the proposed LSTM-based  
 368 model.

Epoch	Hidden nodes	RMSE	$R^2$	Time(min)
100	50	0.0104	0.9902	1.01
	60	0.0098	0.9916	1.38
	70	0.0095	0.9922	1.53
	80	0.01	0.9913	1.75
200	50	0.0094	0.9922	1.91
	60	0.0089	0.9931	2.59
	<b>70</b>	<b>0.0088</b>	<b>0.9932</b>	<b>2.96</b>
	80	0.0092	0.9925	3.28
300	50	0.0101	0.9903	2.86
	60	0.0105	0.9901	3.85
	70	0.0103	0.9907	4.29
	80	0.0120	0.9872	4.92

369



370

371 Figure 6. The variation of RMSE and  $R^2$  values between the observed and predicted  
 372 groundwater levels of well BH01 with the increasing of the number of epochs when the  
 373 hidden node is 50.

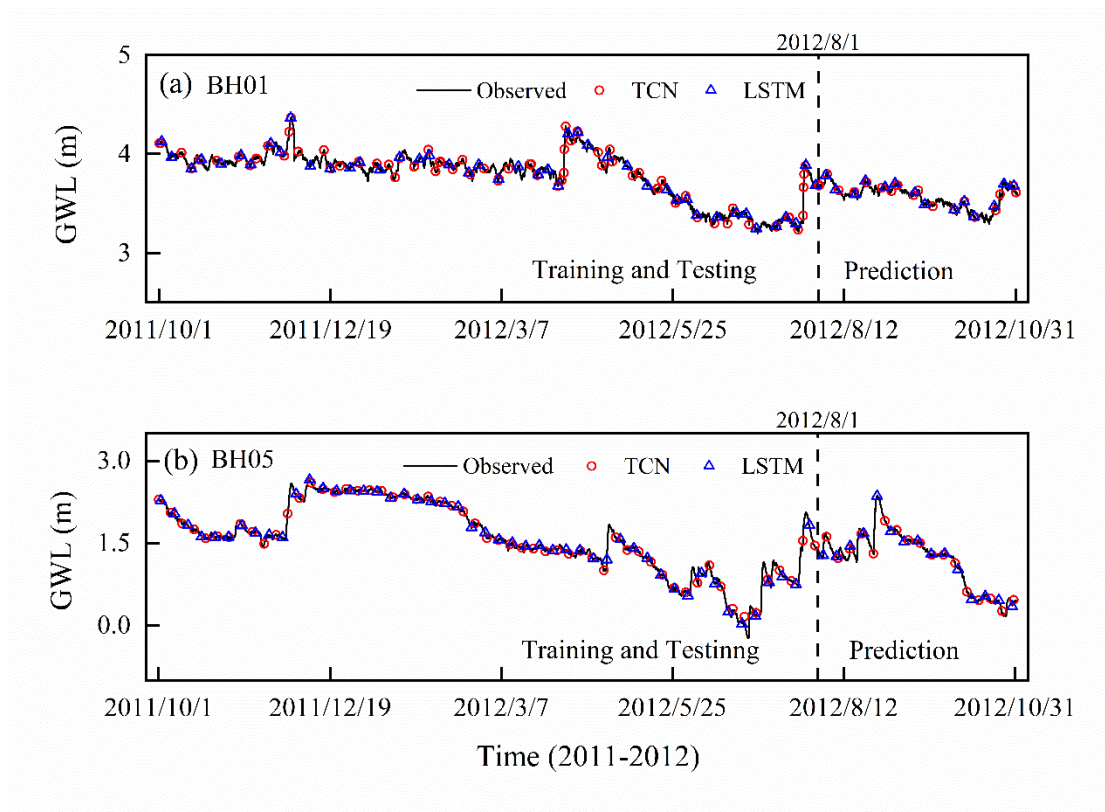
374 The trial experimental results present a similar fitting pattern shared by the two  
375 kinds of networks. The growing value of parameters dramatically increases the  
376 computational cost in the network. For example, the time cost from 50 to 80 hidden  
377 nodes has increased about 1.7 times in each iteration trial in the LSTM-based model.  
378 Finally, 200 epochs, 32 filters, and 16 batch size were chosen as the optimal parameters  
379 in the TCN network. For the LSTM network, the number of epochs and hidden nodes  
380 were chosen as 200 and 70.

### 381 **4.3 Model performance and evaluation**

382 The optimal hyper-parameters of the proposed TCN-based model for  
383 groundwater level predicting are shown in Table 1 (epoch = 200, filters = 32 and batch  
384 size = 16). Besides that, the kernel size in each convolutional layer is set as 6, and the  
385 dilations are [1,2,4,8]. For the LSTM-based model, the batch size is set to 148 with  
386 epoch=200 and nodes=70. The same hyper-parameters are then utilized to construct  
387 TCN and LSTM architectures for the prediction of groundwater level in different  
388 monitoring wells.

389 The one-step-ahead simulated groundwater level in the training and testing and  
390 prediction stages by the two models are shown in Fig. 7. For both models, the simulated  
391 values completely capture the variation of groundwater levels in monitoring wells with  
392 the overlapped plots. The  $R^2$  and RMSE values of simulation results are listed in Table  
393 3. In the prediction stage, the values of RMSE are 0.0019 and 0.0166 for BH01 and  
394 BH05, and the values of  $R^2$  are larger than 0.999 in the prediction for the TCN-based  
395 model. For the LSTM-based model, the RMSE values are 0.0074 and 0.0588, and the

396  $R^2$  values are 0.9957 and 0.9980. These metrics indicate that both models can  
 397 “remember” the historical records and produce true observations. The simulation  
 398 accuracy of TCN-based models is slightly higher than the LSTM-based models. In  
 399 addition, the running time of the TCN-based model is 2.6 minutes, which is faster than  
 400 that of the TCN-based model.



401  
 402 Figure 7. The simulation results of groundwater level of monitoring wells BH01 and  
 403 BH05 by TCN-based model. The black dash line divides the data into two groups: the  
 404 training and testing dataset, and the prediction dataset.

405  
 406 Table 3. The model results for groundwater level in the training and testing and  
 407 prediction stage

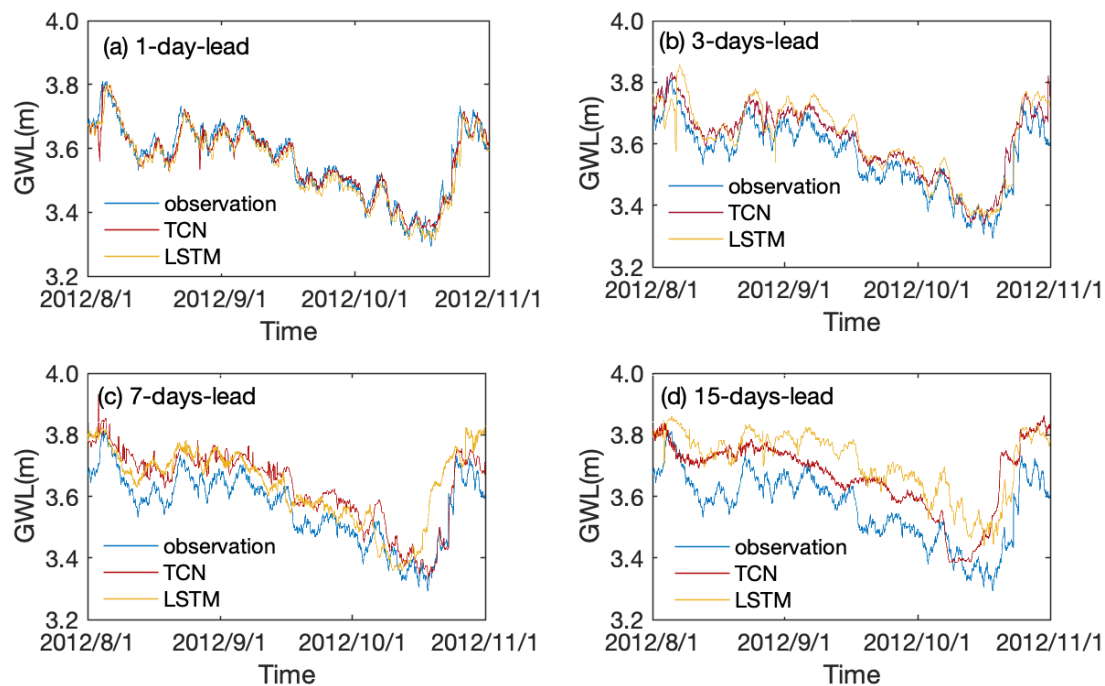
Well	Model	Training and Testing			Prediction		
		MAE	RMSE	$R^2$	MAE	RMSE	$R^2$

BH01	TCN	0.0017	0.0068	0.9992	0.0009	0.0019	0.9997
	LSTM	0.0053	0.0077	0.9990	0.0050	0.0074	0.9957
BH05	TCN	0.0070	0.0279	0.9981	0.0061	0.0166	0.9990
	LSTM	0.0082	0.0116	0.9997	0.0168	0.0558	0.9980

408

#### 409 4.4 Long term leading time prediction

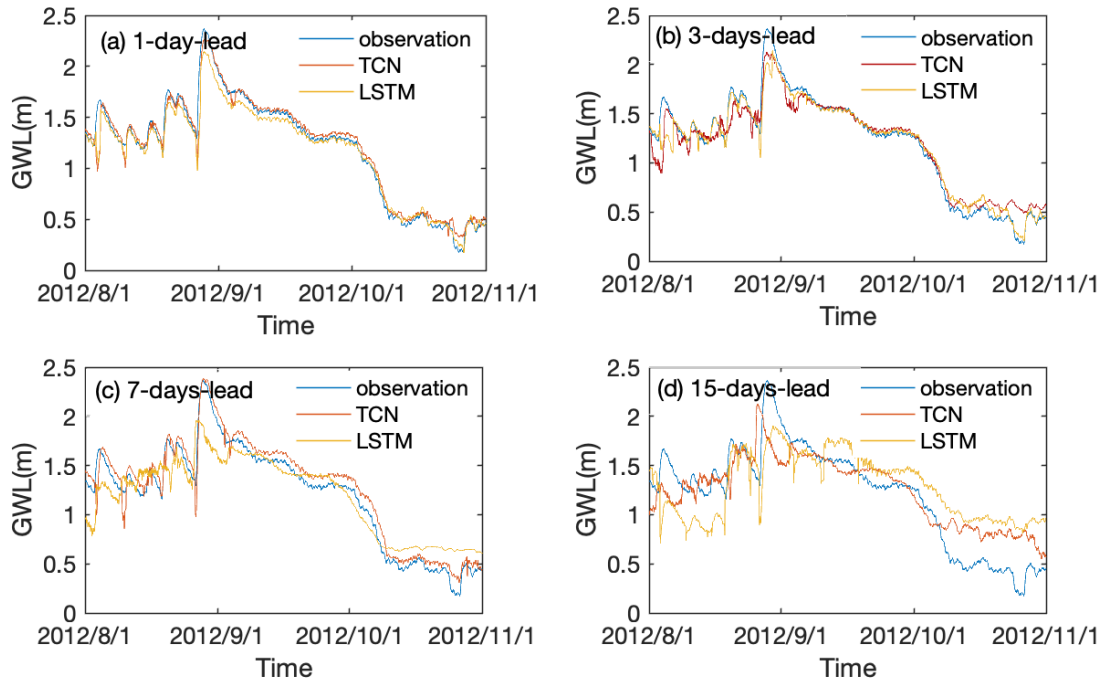
410 The TCN- and LSTM-based models were further adjusted to predict the  
411 groundwater levels over three months ahead with different leading periods. Prediction  
412 results with 1-day, 3-, 7-, and 15-days leading time with TCN- and LSTM-based models  
413 are illustrated in Fig. 8 and Fig. 9 for wells BH01 and BH05, respectively. The results  
414 show that the predicted groundwater values have the same change trend as the actual  
415 groundwater level in monitoring wells. Both of the models are able to capture the  
416 variation trend of groundwater levels with longer leading periods of more than one-  
417 time step in the two monitoring wells.



418

419 Figure 8. The observed and predicted values of the groundwater level with TCN- and

420 LSTM-based models for 1-day, 3-, 7- and 15-days lead period in monitoring well BH01.



421

422 Figure 9. The observed and predicted values of the groundwater level with TCN- and  
423 LSTM-based models for 1-day, 3-, 7-, and 15-days leading period in monitoring well  
424 BH05.

425 To quantitatively compare the prediction accuracy of the proposed TCN- and  
426 LSTM-based models, the results of two evaluation metrics with the model running time  
427 are summarized in Table 4. It can be learned that the  $R^2$  value of TCN-based models  
428 decreased from 0.9386 to -0.1407 for well BH01 and from 0.9670 to 0.7271 for well  
429 BH05. Correspondingly, an increase of RMSE values from 0.028 to 0.1209 and 0.0934  
430 to 0.206 are observed for BH01 and BH05, separately. A similar variation pattern is  
431 recognized for the LSTM-based model with smaller  $R^2$  and higher RMSE than that of  
432 the TCN-based model. Notably, the running time of advance prediction is much longer  
433 than that of single-step prediction. Meanwhile, with the increasing of the leading period,  
434 the time had been raised nonlinearly. Further, in this process, the TCN-based model

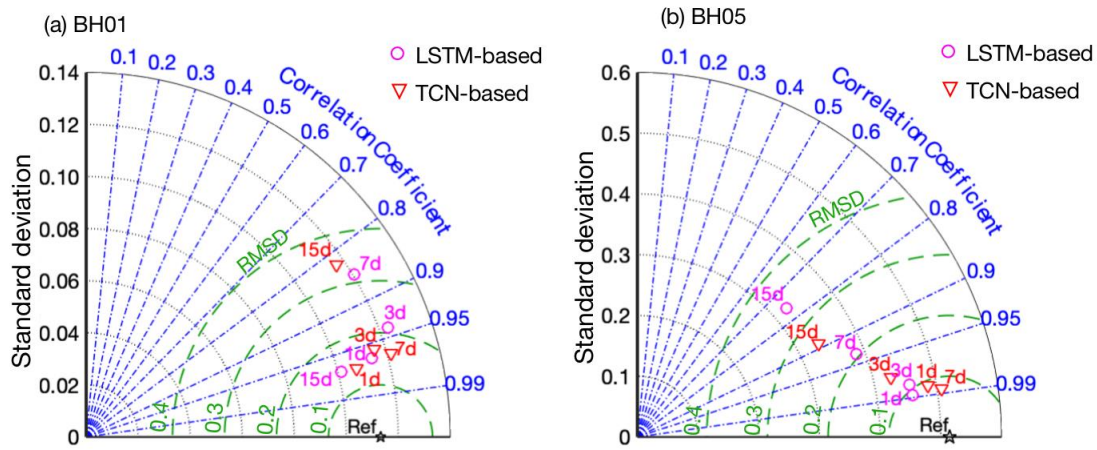


435 costs longer time than that of the LSTM-based model.

436 Table 4. The model results for groundwater level in the long-term prediction

Well	Model	Prediction		Mins	Model	Prediction		Mins
		RMSE	R <sup>2</sup>			RMSE	R <sup>2</sup>	
BH01	TCN-1	0.0280	0.9386	5.38	LSTM-1	0.0349	0.9047	3.76
	TCN-3	0.0550	0.7638	16.1	LSTM-3	0.0640	0.6802	11.01
	TCN-7	0.0741	0.5713	34.3	LSTM-7	0.0956	0.2874	26.27
	TCN-15	0.1209	-0.1407	94.95	LSTM-15	0.1486	-0.7227	85.13
BH05	TCN-1	0.0934	0.9670	5.19	LSTM-1	0.1012	0.9613	3.78
	TCN-3	0.1375	0.9285	16.18	LSTM-3	0.1086	0.9554	11.4
	TCN-7	0.1084	0.9296	35.44	LSTM-7	0.2050	0.8406	26.2
	TCN-15	0.2060	0.7271	80.46	LSTM-15	0.3515	0.5330	73.45

437 The performance of the two networks was further evaluated with Taylor diagrams  
 438 by taking different criteria aspects, including standard deviation (SD), correlation  
 439 coefficient (COR), and root mean square deviation (RMSD) into account (Taylor, 2001).  
 440 The comparisons of the TCN- and LSTM-based models are shown in Fig. 10. As the  
 441 metrics are distributed away from the reference point (Ref), the deviation of prediction  
 442 from observation is generally increased with extending of the leading period. Taking  
 443 well BH05 for example, the prediction with 1-day (24 hours prediction window) in  
 444 advance is the highest in agreement with the actual situation in the two models. The 1-  
 445 day leading prediction results have the lowest RMSD values and highest R<sup>2</sup> values for  
 446 both models. The prediction precision gradually decreases with the extension of leading  
 447 time to 3-days, 7-days, and 15-days. For well BH01, an out-of-trending point is  
 448 observed. The 15-day prediction results of the LSTM-based model are closer to the Ref  
 449 point compared with the TCN-based model. The reason is that the simulation data is  
 450 highly correlated with observations as shown in Fig. 8.



451

452 Figure 10. Taylor diagrams with statistical (SD, COR, RMSD) comparison results of  
 453 the TCN-based and LSTM-based models for well (a) BH01, (b) BH05.

454 Overall, the TCN- and LSTM-based models both have strong prediction abilities  
 455 in long-term hydrological time series data. Both models are able to provide accurate  
 456 predictions once they are trained. The simulation accuracy of the TCN-based model is  
 457 slightly better than that of the LSTM-based model in the three months prediction but  
 458 the difference is not significant, with  $p > 0.05$  in the t-test. The causal dilated  
 459 convolutions used by TCNs are proven to be good at capturing long-term dependencies  
 460 of time series data. Meanwhile, the model precision decreases and the running time  
 461 increases with the raising leading period. The processing speed of parallel convolution  
 462 TCN-based models for long input sequences is slower than that of recurrent networks.  
 463 This seems to be a shortage in real-time monitoring and early warning. A leading period  
 464 shorter than 7 days is recommended to ensure both the accuracy and efficiency of the  
 465 models in real-time monitoring and early warning.

466 From the groundwater level variation, significant groundwater decreasing trends  
 467 can be observed in the irrigation season from March to June. Therefore, human

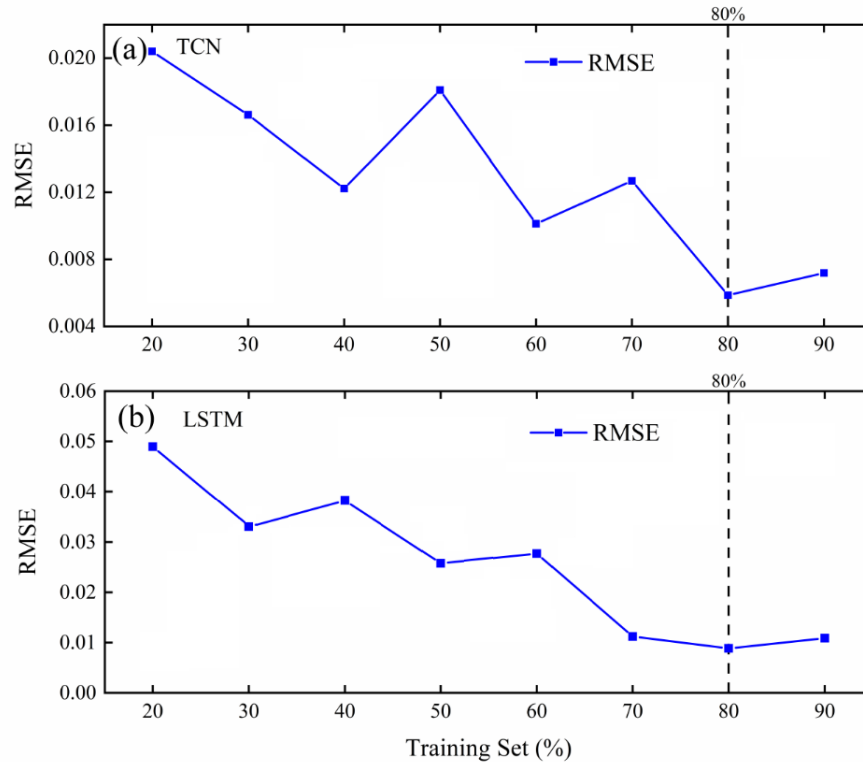
468 activities, such as groundwater pumping are potential reasons for groundwater level  
469 change in the study area. Here, the groundwater levels were predicted based on the  
470 available data of precipitation and tide. If the pumping data is available and  
471 considered in the models, the prediction precision would be enhanced in the models.

#### 472 **4.5 Influence of training set percentage**

473 The data-driven methods are supported by data; however, how much data is needed  
474 to build an effective model is still a challenging problem (Reichstein et al., 2019). This  
475 is because specific problems depend on application cases, data features, and model  
476 features (Wunsch et al., 2021). Here we discuss the effect of the training set percentage  
477 on the TCN- and LSTM-based models. In our study, the data is the hourly-monitored  
478 data from 2011 to 2012. From 2011, we set 20%, 30% to 90% training sets in turn, so  
479 as to gradually expand the length of the training set.

480 Fig. 11 shows the effect of the increased percentage of the training set on the  
481 performance of the model. All experiments were repeated five times, and the average  
482 values of each index were compared. It can be seen that the performance of the TCN-  
483 based model improved with the increase of the percentage of the training set. When the  
484 training set reached 80%, the performance was relatively optimal, and then the  
485 performance began to deteriorate with the increase of the percentage of the training set.  
486 At the same time, it can be seen that the performance of the LSTM-based model tends  
487 to be stable when the training set reaches 70%, and then decreases slightly with the  
488 increase of the training set. Therefore, a training set evaluation is recommended before  
489 the training and testing. We should carefully evaluate and shorten the training data set

490 as much as possible when necessary. Finally, we set 80% of the training set length to  
491 simulate the coastal aquifer time-series data.



492

493 Figure 11. Influence of training set percentage on the performance of the model for (a)  
494 BH01 and (b) BH05.

## 495 5 Conclusions

496 The TCN- and LSTM-based deep learning models were proposed in this paper to  
497 predict groundwater levels in a coastal aquifer. Hyper-parameter searches were first  
498 conducted to obtain good architecture configurations. The results indicated that a deeper,  
499 broader model does not necessarily guarantee better predictions. The optimal  
500 configurations were then adopted for the networks of all monitoring data. Both the  
501 TCN- and LSTM- based models well captured the fluctuation of groundwater levels  
502 and achieved satisfactory performance on the prediction. Meanwhile, a decreasing

503 precision is revealed when the leading time increases in advance prediction. In view of  
504 accuracy, the TCN-based model outperforms the LSTM-based model but is less  
505 efficient in long-term simulation. Thus, both models can be used as a promising method  
506 for time-series prediction of hydrogeological data, especially when the regional data is  
507 difficult to collect in a complex system.

### 508 **Acknowledgements**

509 This work was jointly supported by National Natural Science Foundation of  
510 China (No: 41702244), the Program for Jilin University (JLU) Science and Technology  
511 Innovative Research Team (No. 2019TD-35).

### 512 **Code availability**

513 The pieces of code that were used for all analyses are available from the authors  
514 upon request.

### 515 **Data availability**

516 The data sets that have been analyzed in this paper are available from the  
517 authors upon request.

### 518 **Author contribution**

519 XZ drafted the manuscript and revised the manuscript. GC designed the  
520 experiments and collected all the data. DF developed the model code and performed  
521 the simulations. ZD was responsible for the project design, oversaw the analysis, and  
522 conducted manuscript revision as the project leader and the senior scientist.

### 523 **Competing interests**

524 The authors declare that they have no conflict of interest.

525 **Reference**

- 526 Abdalla, O. A. and Al-Rawahi, A. S.: Groundwater recharge dams in arid areas as tools  
527 for aquifer replenishment and mitigating seawater intrusion: example of AlKhod,  
528 Oman, *Environ. Earth Sci.*, 69, 1951-1962, 2013.
- 529 Adam, D. K. J. B.: A method for stochastic optimization in: 3rd International  
530 Conference on Learning Representations, 2015.
- 531 Afaq, S. and Rao, S.: Significance of epochs on training a neural network, *International*  
532 *Journal of Scientific & Technology Research*, 9, 485-488, 2020.
- 533 Baena-Ruiz, L., Pulido-Velazquez, D., Collados-Lara, A.-J., Renau-Pruñonosa, A., and  
534 Morell, I.: Global assessment of seawater intrusion problems (status and  
535 vulnerability), *Water Resour. Manag.*, 32, 2681-2700, 2018.
- 536 Bai, S., Kolter, J. Z., and Koltun, V.: An empirical evaluation of generic convolutional  
537 and recurrent networks for sequence modeling, arXiv preprint arXiv:1803.01271,  
538 2018.
- 539 Barlow, P. M. and Reichard, E. G.: Saltwater intrusion in coastal regions of North  
540 America, *Hydrogeol. J.*, 18, 247-260, 2010.
- 541 Batelaan, O., De Smedt, F., and Triest, L.: Regional groundwater discharge:  
542 phreatophyte mapping, groundwater modelling and impact analysis of land-use  
543 change, *J. Hydrol.*, 275, 86-108, 2003.
- 544 Bengio, Y., Simard, P., and Frasconi, P.: Learning long-term dependencies with gradient  
545 descent is difficult, *IEEE Trans. Neural Netw.*, 5, 157-166, 1994.
- 546 Borovykh, A., Bohte, S., and Oosterlee, C. W.: Dilated convolutional neural networks  
547 for time series forecasting, *J. Comput. Financ.*, 2018.
- 548 Cannas, B., Fanni, A., See, L., and Sias, G.: Data preprocessing for river flow  
549 forecasting using neural networks: wavelet transforms and data partitioning, *Phys.*  
550 *Chem. Earth*, 31, 1164-1171, 2006.
- 551 Cao, Y., Ding, Y., Jia, M., and Tian, R.: A novel temporal convolutional network with  
552 residual self-attention mechanism for remaining useful life prediction of rolling  
553 bearings, *Reliab. Eng. Syst. Saf.*, 215, 107813, 2021.
- 554 Chen, Y., Kang, Y., Chen, Y., and Wang, Z.: Probabilistic forecasting with temporal  
555 convolutional neural network, *Neurocomputing*, 399, 491-501, 2020.
- 556 Coulibaly, P., Anctil, F., Aravena, R., and Bobée, B.: Artificial neural network modeling  
557 of water table depth fluctuations, *Water Resour. Res.*, 37, 885-896, 2001.
- 558 Dai, Z. and Samper, J.: Inverse modeling of water flow and multicomponent reactive  
559 transport in coastal aquifer systems, *J. Hydrol.*, 327, 447-461, 2006.
- 560 Dai, Z., Xu, L., Xiao, T., McPherson, B., Zhang, X., Zheng, L., Dong, S., Yang, Z.,  
561 Soltanian, M. R., and Yang, C.: Reactive chemical transport simulations of geologic  
562 carbon sequestration: Methods and applications, *Earth-Sci. Rev.*, 208, 103265, 2020.
- 563 Dubey, A. K., Kumar, A., García-Díaz, V., Sharma, A. K., and Kanhaiya, K.: Study and  
564 analysis of SARIMA and LSTM in forecasting time series data, *Sustain. Energy*  
565 *Technol. Assess.*, 47, 101474, 2021.
- 566 Ergen, T. and Kozat, S. S.: Efficient online learning algorithms based on LSTM neural  
567 networks, *IEEE Trans. Neural Netw. Learn. Syst.*, 29, 3772-3783, 2017.

568 Feng, N., Geng, X., and Qin, L.: Study on MRI medical image segmentation technology  
569 based on CNN-CRF model, *IEEE Access*, 8, 60505-60514, 2020.

570 Fischer, T. and Krauss, C.: Deep learning with long short-term memory networks for  
571 financial market predictions, *Eur. J. Oper. Res.*, 270, 654-669, 2018.

572 Gan, Z., Li, C., Zhou, J., and Tang, G.: Temporal convolutional networks interval  
573 prediction model for wind speed forecasting, *Electr. Power Syst. Res.*, 191, 106865,  
574 2021.

575 Garza-Díaz, L. E., DeVincentis, A. J., Sandoval-Solis, S., Azizipour, M., Ortiz-Partida,  
576 J. P., Mahlknecht, J., Cahn, M., Medellín-Azuara, J., Zaccaria, D., and Kisekka, I.:  
577 Land-use optimization for sustainable agricultural water management in Pajaro  
578 Valley, California, *J. Water Resour. Plan. Manage.-ASCE*, 145, 05019018-  
579 05019018, 2019.

580 Gorgij, A. D., Kisi, O., and Moghaddam, A. A.: Groundwater budget forecasting, using  
581 hybrid wavelet-ANN-GP modelling: a case study of Azarshahr Plain, East  
582 Azerbaijan, Iran, *Hydrol. Res.*, 48, 455-467, 2017.

583 Han, D., Kohfahl, C., Song, X., Xiao, G., and Yang, J.: Geochemical and isotopic  
584 evidence for palaeo-seawater intrusion into the south coast aquifer of Laizhou Bay,  
585 China, *Appl. Geochem.*, 26, 863-883, 2011.

586 Han, D., Song, X., Currell, M. J., Yang, J., and Xiao, G.: Chemical and isotopic  
587 constraints on evolution of groundwater salinization in the coastal plain aquifer of  
588 Laizhou Bay, China, *J. Hydrol.*, 508, 12-27, 2014.

589 He, K., Zhang, X., Ren, S., and Sun, J.: Deep residual learning for image recognition,  
590 *Proc. IEEE*, 770-778,

591 Huang, F.-K., Chuang, M.-H., Wang, G. S., and Yeh, H.-D.: Tide-induced groundwater  
592 level fluctuation in a U-shaped coastal aquifer, *J. Hydrol.*, 530, 291-305, 2015.

593 Jiang, Y., Zhao, M., Zhao, W., Qin, H., Qi, H., Wang, K., and Wang, C.: Prediction of  
594 sea temperature using temporal convolutional network and LSTM-GRU network,  
595 *Complex Engineering Systems*, 1, -, 2021.

596 Ketabchi, H. and Ataie-Ashtiani, B.: Evolutionary algorithms for the optimal  
597 management of coastal groundwater: A comparative study toward future challenges,  
598 *J. Hydrol.*, 520, 193-213, 2015.

599 Kratzert, F., Herrnegger, M., Klotz, D., Hochreiter, S., and Klambauer, G.:  
600 NeuralHydrology—interpreting LSTMs in hydrology, in: *Explainable AI:  
601 Interpreting, explaining and visualizing deep learning*, Springer, 347-362, 2019.

602 Kreyenberg, P. J., Bauser, H. H., and Roth, K.: Velocity field estimation on density-  
603 driven solute transport with a convolutional neural network, *Water Resour. Res.*, 55,  
604 7275-7293, 2019.

605 Lara-Benítez, P., Carranza-García, M., Luna-Romera, J. M., and Riquelme, J. C.:  
606 Temporal convolutional networks applied to energy-related time series forecasting,  
607 *applied sciences*, 10, 2322, 2020.

608 Lea, C., Vidal, R., Reiter, A., and Hager, G. D.: Temporal convolutional networks: A  
609 unified approach to action segmentation, *European conference on computer vision*,  
610 47-54,

611 Lea, C., Flynn, M. D., Vidal, R., Reiter, A., and Hager, G. D.: Temporal convolutional

612 networks for action segmentation and detection, Proc. IEEE, 156-165,  
613 LeCun, Y., Bottou, L., Bengio, Y., and Haffner, P.: Gradient-based learning applied to  
614 document recognition, Proc. IEEE, 86, 2278-2324, 1998.  
615 Li, H., Jiao, J. J., Luk, M., and Cheung, K.: Tide-induced groundwater level fluctuation  
616 in coastal aquifers bounded by L-shaped coastlines, Water Resour. Res., 38, 6-1-6-  
617 8, 2002.  
618 Long, J., Shelhamer, E., and Darrell, T.: Fully convolutional networks for semantic  
619 segmentation, Proc. IEEE, 3431-3440,  
620 Lu, C., Werner, A. D., and Simmons, C. T.: Threats to coastal aquifers, Nature Climate  
621 Change, 3, 605-605, 2013.  
622 Lu, C., Cao, H., Ma, J., Shi, W., Rathore, S. S., Wu, J., and Luo, J.: A proof-of-concept  
623 study of using a less permeable slice along the shoreline to increase fresh  
624 groundwater storage of oceanic islands: Analytical and experimental validation,  
625 Water Resour. Res., 55, 6450-6463, 2019.  
626 Maier, H. R. and Dandy, G. C.: Neural networks for the prediction and forecasting of  
627 water resources variables: a review of modelling issues and applications, Environ.  
628 Modell. Softw., 15, 101-124, 2000.  
629 Mehr, A. D. and Nourani, V.: A Pareto-optimal moving average-multigene genetic  
630 programming model for rainfall-runoff modelling, Environ. Modell. Softw., 92,  
631 239-251, 2017.  
632 Mei, Y., Tan, G., and Liu, Z.: An improved brain-inspired emotional learning algorithm  
633 for fast classification, Algorithms, 10, 70, 2017.  
634 Nair, V. and Hinton, G. E.: Rectified linear units improve restricted boltzmann machines,  
635 Icml,  
636 Park, Y., Lee, J.-Y., Kim, J.-H., and Song, S.-H.: National scale evaluation of  
637 groundwater chemistry in Korea coastal aquifers: evidences of seawater intrusion,  
638 Environ. Earth Sci., 66, 707-718, 2012.  
639 Pascanu, R., Mikolov, T., and Bengio, Y.: On the difficulty of training recurrent neural  
640 networks, International conference on machine learning, 1310-1318, 2013.  
641 Pratheepa, V., Ramesh, S., Sukumaran, N., and Murugesan, A.: Identification of the  
642 sources for groundwater salinization in the coastal aquifers of Southern Tamil Nadu,  
643 India, Environ. Earth Sci., 74, 2819-2829, 2015.  
644 Reichstein, M., Camps-Valls, G., Stevens, B., Jung, M., Denzler, J., and Carvalhais, N.:  
645 Deep learning and process understanding for data-driven Earth system science,  
646 Nature, 566, 195-204, 2019.  
647 Rumelhart, D. E., Hinton, G. E., and Williams, R. J.: Learning representations by back-  
648 propagating errors, Nature, 323, 533-536, 1986.  
649 Sahoo, S., Russo, T., Elliott, J., and Foster, I.: Machine learning algorithms for  
650 modeling groundwater level changes in agricultural regions of the US, Water Resour.  
651 Res., 53, 3878-3895, 2017.  
652 Salimans, T. and Kingma, D. P.: Weight normalization: A simple reparameterization to  
653 accelerate training of deep neural networks, Advances in neural information  
654 processing systems, 29, 2016.  
655 Senthil Kumar, A., Sudheer, K., Jain, S., and Agarwal, P.: Rainfall-runoff modelling



656 using artificial neural networks: comparison of network types, *Hydrological*  
657 *Processes: An International Journal*, 19, 1277-1291, 2005.

658 Seo, Y., Kim, S., Kisi, O., and Singh, V. P.: Daily water level forecasting using wavelet  
659 decomposition and artificial intelligence techniques, *J. Hydrol.*, 520, 224-243, 2015.

660 Solgi, R., Loáiciga, H. A., and Kram, M.: Long short-term memory neural network  
661 (LSTM-NN) for aquifer level time series forecasting using in-situ piezometric  
662 observations, *J. Hydrol.*, 601, 126800, 2021.

663 Srivastava, N., Hinton, G., Krizhevsky, A., Sutskever, I., and Salakhutdinov, R.:  
664 Dropout: a simple way to prevent neural networks from overfitting, *J. Mach. Learn.*  
665 *Res.*, 15, 1929-1958, 2014.

666 Taylor, K. E.: Summarizing multiple aspects of model performance in a single diagram,  
667 *J. Geophys. Res.-Atmos.*, 106, 7183-7192, 2001.

668 Torres, J. F., Troncoso, A., Koprinska, I., Wang, Z., and Martínez-Álvarez, F.: Deep  
669 learning for big data time series forecasting applied to solar power, *The 13th*  
670 *International Conference on Soft Computing Models in Industrial and*  
671 *Environmental Applications*, 123-133, 2018.

672 Wan, R., Mei, S., Wang, J., Liu, M., and Yang, F.: Multivariate temporal convolutional  
673 network: A deep neural networks approach for multivariate time series forecasting,  
674 *Electronics*, 8, 876, 2019.

675 Wunsch, A., Liesch, T., and Broda, S.: Groundwater level forecasting with artificial  
676 neural networks: a comparison of long short-term memory (LSTM), convolutional  
677 neural networks (CNNs), and non-linear autoregressive networks with exogenous  
678 input (NARX), *Hydrol. Earth Syst. Sci.*, 25, 1671-1687, 2021.

679 Xu, Z. and Hu, B. X.: Development of a discrete-continuum VDFST-CFP numerical  
680 model for simulating seawater intrusion to a coastal karst aquifer with a conduit  
681 system, *Water Resour. Res.*, 53, 688-711, 2017.

682 Xue, Y., Wu, J., Ye, S., and Zhang, Y.: Hydrogeological and hydrogeochemical studies  
683 for salt water intrusion on the south coast of Laizhou Bay, China, *Groundwater*, 38,  
684 38-45, 2000.

685 Yan, J., Mu, L., Wang, L., Ranjan, R., and Zomaya, A. Y.: Temporal convolutional  
686 networks for the advance prediction of ENSO, *Sci Rep*, 10, 1-15, 2020.

687 Zeng, X., Wu, J., Wang, D., and Zhu, X.: Assessing the pollution risk of a groundwater  
688 source field at western Laizhou Bay under seawater intrusion, *Environ. Res.*, 148,  
689 586-594, 2016.

690 Zhan, C., Dai, Z., Soltanian, M. R., and Zhang, X.: Stage-wise stochastic deep learning  
691 inversion framework for subsurface sedimentary structure identification, *Geophys.*  
692 *Res. Lett.*, 49, e2021GL095823, 2022.

693 Zhang, D., Lin, J., Peng, Q., Wang, D., Yang, T., Sorooshian, S., Liu, X., and Zhuang,  
694 J.: Modeling and simulating of reservoir operation using the artificial neural  
695 network, support vector regression, deep learning algorithm, *J. Hydrol.*, 565, 720-  
696 736, 2018a.

697 Zhang, J., Zhu, Y., Zhang, X., Ye, M., and Yang, J.: Developing a Long Short-Term  
698 Memory (LSTM) based model for predicting water table depth in agricultural areas,  
699 *J. Hydrol.*, 561, 918-929, 2018b.

700 Zhang, J., Zhang, X., Niu, J., Hu, B. X., Soltanian, M. R., Qiu, H., and Yang, L.:  
701 Prediction of groundwater level in seashore reclaimed land using wavelet and  
702 artificial neural network-based hybrid model, *J. Hydrol.*, 577, 123948, 2019.  
703 Zhang, X., Miao, J., Hu, B. X., Liu, H., Zhang, H., and Ma, Z.: Hydrogeochemical  
704 characterization and groundwater quality assessment in intruded coastal brine  
705 aquifers (Laizhou Bay, China), *Environ. Sci. Pollut. Res.*, 24, 21073-21090, 2017.  
706 Zhang, X., Dong, F., Dai, H., Hu, B. X., Qin, G., Li, D., Lv, X., Dai, Z., and Soltanian,  
707 M. R.: Influence of lunar semidiurnal tides on groundwater dynamics in estuarine  
708 aquifers, *Hydrogeol. J.*, 28, 1419-1429, 2020.  
709